Blockade of Endothelial-Mesenchymal Transition by a Smad3 Inhibitor Delays the Early Development of Streptozotocin-Induced Diabetic Nephropathy

Jinhua Li,[1] Xinli Qu,[1] Jun Yao,[1] Georgina Caruana,[1] Sharon D. Ricardo,[2] Yasuhiko Yamamoto,[3] Hiroshi Yamamoto,[3] and John F. Bertram[1]

OBJECTIVE—A multicenter, controlled trial showed that early blockade of the renin-angiotensin system in patients with type 1 diabetes and normoalbuminuria did not retard the progression of nephropathy, suggesting that other mechanism(s) are involved in the pathogenesis of early diabetic nephropathy (diabetic nephropathy). We have previously demonstrated that endothelial-mesenchymal-transition (EndoMT) contributes to the early development of renal interstitial fibrosis independently of microalbuminuria in mice with streptozotocin (STZ)-induced diabetes. In the present study, we hypothesized that blocking EndoMT reduces the early development of diabetic nephropathy.

RESEARCH DESIGN AND METHODS—EndoMT was induced in a mouse pancreatic microvascular endothelial cell line (MMEC) in the presence of advanced glycation end products (AGEs) and in the endothelial lineage–traceble mouse line *Tie2-Cre;Loxp-EGFP* by administration of AGEs, with nonglycated mouse albumin serving as a control. Phosphorylated Smad3 was detected by immunoprecipitation/Western blotting and confocal microscopy. Blocking studies using receptor for AGE siRNA and a specific inhibitor of Smad3 (SIS3) were performed in MMECs and in STZ-induced diabetic nephropathy in *Tie2-Cre;Loxp-EGFP* mice.

RESULTS—Confocal microscopy and real-time PCR demonstrated that AGEs induced EndoMT in MMECs and in *Tie2-Cre;Loxp-EGFP* mice. Immunoprecipitation/Western blotting showed that Smad3 was activated by AGEs but was inhibited by SIS3 in MMECs and in STZ-induced diabetic nephropathy. Confocal microscopy and real-time PCR further demonstrated that SIS3 abrogated EndoMT, reduced renal fibrosis, and retarded progression of nephropathy.

CONCLUSIONS—EndoMT is a novel pathway leading to early development of diabetic nephropathy. Blockade of EndoMT by SIS3 may provide a new strategy to retard the progression of diabetic nephropathy and other diabetes complications. ***Diabetes*** **59:2612–2624, 2010**

From the [1]Department of Anatomy and Developmental Biology, Monash University, Victoria, Australia; [2]Monash Immunology and Stem Cell Laboratories, Monash University, Victoria, Australia; and the [3]Department of Biochemistry and Molecular Vascular Biology, Kanazawa University Graduate School of Medical Science, Kanazawa, Japan.

Corresponding author: Jinhua Li, jinhua.li@med.monash.edu.au.

Received 4 November 2009 and accepted 9 July 2010. Published ahead of print at http://diabetes.diabetesjournals.org on 3 August 2010. DOI: 10.2337/db09-1631.

Diabetic nephropathy is a major microvascular complication of both type 1 and type 2 diabetes. Increased glomerular basement membrane thickness, mesangial expansion, glomerular sclerosis, and tubulointerstitial fibrosis are major features of diabetic nephropathy. The severity of glomerulosclerosis and tubulointerstitial fibrosis are strong predictors of the progression to end-stage renal disease, making this an important therapeutic target.

Current clinical treatment guidelines for diabetic nephropathy include the control of hyperfiltration, microalbuminuria, systemic blood pressure, and blood glucose (1). Multiple clinical trials have shown that blockade of the renin-angiotensin system (RAS) can improve renal function in late diabetic nephropathy in patients with proteinuria, diabetes, and reduced glomerular filtration rate (2–4). Recently, however, a large-scale multicenter controlled trial revealed that inhibition of the RAS in normotensive patients with type 1 diabetes and normoalbuminuria did not reduce the incidence of microalbuminuria or slow the decline of renal function, suggesting that the pathogenesis of early diabetic nephropathy may differ from that of late diabetic renal disease (5).

Myofibroblasts are major contributors to extracellular matrix (ECM) accumulation in fibrotic disease, and their numbers inversely correlate with renal function in diabetic nephropathy (6,7). It is generally believed that myofibroblasts can be derived from renal fibroblasts, tubular epithelial cells, mesangial cells, and bone marrow–derived cells. Recently, Zeisberg et al. (8) showed that endothelial-mesenchymal-transition (EndoMT) contributed to cardiac fibrosis. They further demonstrated that 30–50% of fibroblasts in three different mouse models of renal disease (unilateral ureteral obstructive [UUO] nephropathy, streptozotocin [STZ]-induced diabetic nephropathy, and a mouse model of Alport syndrome) coexpressed the endothelial marker CD31 and the fibroblast/myofibroblast markers fibroblast specific protein-1 and/or α-smooth muscle actin (α-SMA) (9) . We also recently demonstrated that 10–24% of renal interstitial myofibroblasts in 1- and 6-month STZ-induced diabetic kidneys were of endothelial origin, revealing the existence of EndoMT in the development and progression of diabetic nephropathy (10). However, it is unclear whether blockade of EndoMT can reduce renal fibrosis and retard the early development of diabetic nephropathy.

There is increasing evidence of a causal role for advanced glycation end products (AGEs) in the development of diabetes complications, including nephropathy and vasculopathy (11,12). AGEs exert their effects through the

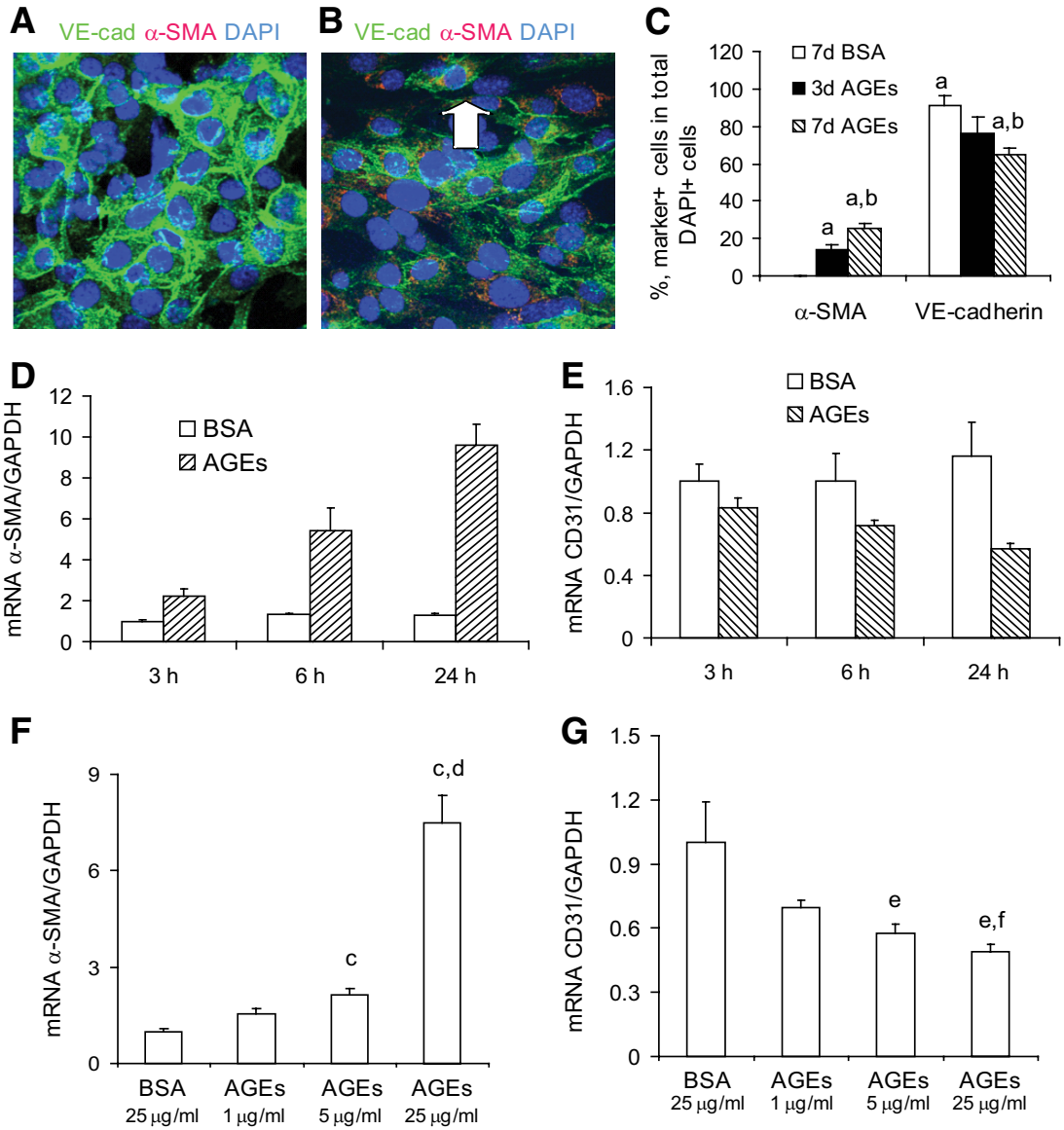

FIG. 1. AGEs induced EndoMT in MMECs. MMECs were cultured in the presence of AGEs (25 μg/ml) or BSA (25 μg/ml) for 3 and 7 days (3d AGEs, 7d BSA, and 7d AGEs). Confocal microscopy demonstrated the expression of VE-cadherin (green), α-SMA (red), and DAPI nuclear staining (blue) in MMECs after culture with either BSA (*A*) or AGEs (*B*) for 7 days. Arrow indicates a VE-cadherin$^+$/α-SMA$^+$ cell. *C*: Quantitation of the percentages of VE-cadherin– and α-SMA–positive cells in total DAPI-positive cells. One-way ANOVA, a, vs. 7d BSA, b ($P < 0.05$) b, vs. 3d AGEs ($P < 0.05$). Real-time PCR demonstrated mRNA levels of α-SMA (*D* and *F*) and CD31 (*E* and *G*) in MMECs cultured in the presence of BSA or AGEs for 3, 6, and 24 h (*D* and *E*) and with different concentrations of AGEs and BSA for 24 h (*F* and *G*). *D*: Two-way ANOVA, time, $P < 0.05$; treatment, $P < 0.05$; interaction, $P < 0.05$. *E*: Two-way ANOVA, time, $P > 0.05$; treatment, $P < 0.05$; interaction, $P < 0.05$. *F*: c, vs. 25 μg/ml BSA or 1 μg/ml AGEs, $P < 0.05$; d, vs. 5 μg/ml AGEs, $P < 0.05$. *G*: e, vs. 25 μg/ml BSA or 1 μg/ml AGEs, $P < 0.05$; f, vs. 5 μg/ml AGEs, $P < 0.05$. (A high-quality digital representation of this figure is available in the online issue.)

formation of protein cross-links that alter the structure and function of ECM and by interacting with specific cell surface receptors (11). The best-characterized AGE receptor is receptor for AGEs (RAGE), although other AGE-binding sites have been identified (12). Disruption of the RAGE gene ameliorates development and progression of diabetic nephropathy (13). AGEs have also been shown to cause epithelial-mesenchymal transdifferentiation via RAGE in diabetic nephropathy (14). It is unknown whether AGEs can induce EndoMT and, if they can, whether blockade of AGE-induced EndoMT can ameliorate the development and progression of diabetic renal fibrosis.

The interaction of AGEs and RAGE on endothelial cells induces cellular oxidant stress and initializes serial signaling pathway activation, including the nuclear factor-κB, extracellular signal–regulated kinase 1 and 2 (ERK1/2), p38 mitogen-activated protein kinase (MAPK), stress-activated protein kinase/c-Jun–NH_2-terminal kinase (SAPK/JNK) and the small GTPase Ras, ρ-family small GTPase Cdc42, and Rac1 pathways (15–23). AGEs also induce rapid and transient activation of Smad2 and Smad3 in tubular epithelial cells, mesangial cells, and vascular smooth muscle cells through RAGE-Smad2/3 cross-talk (24). Whether AGEs can induce Smad3 activation in renal endothelial cells and whether blockade of RAGE-Smad3 cross-talk abrogates AGE-induced EndoMT requires further investigation.

Smad3 plays an essential role in renal fibrosis. Smad3 conditional knockout mice have been shown to be resis-

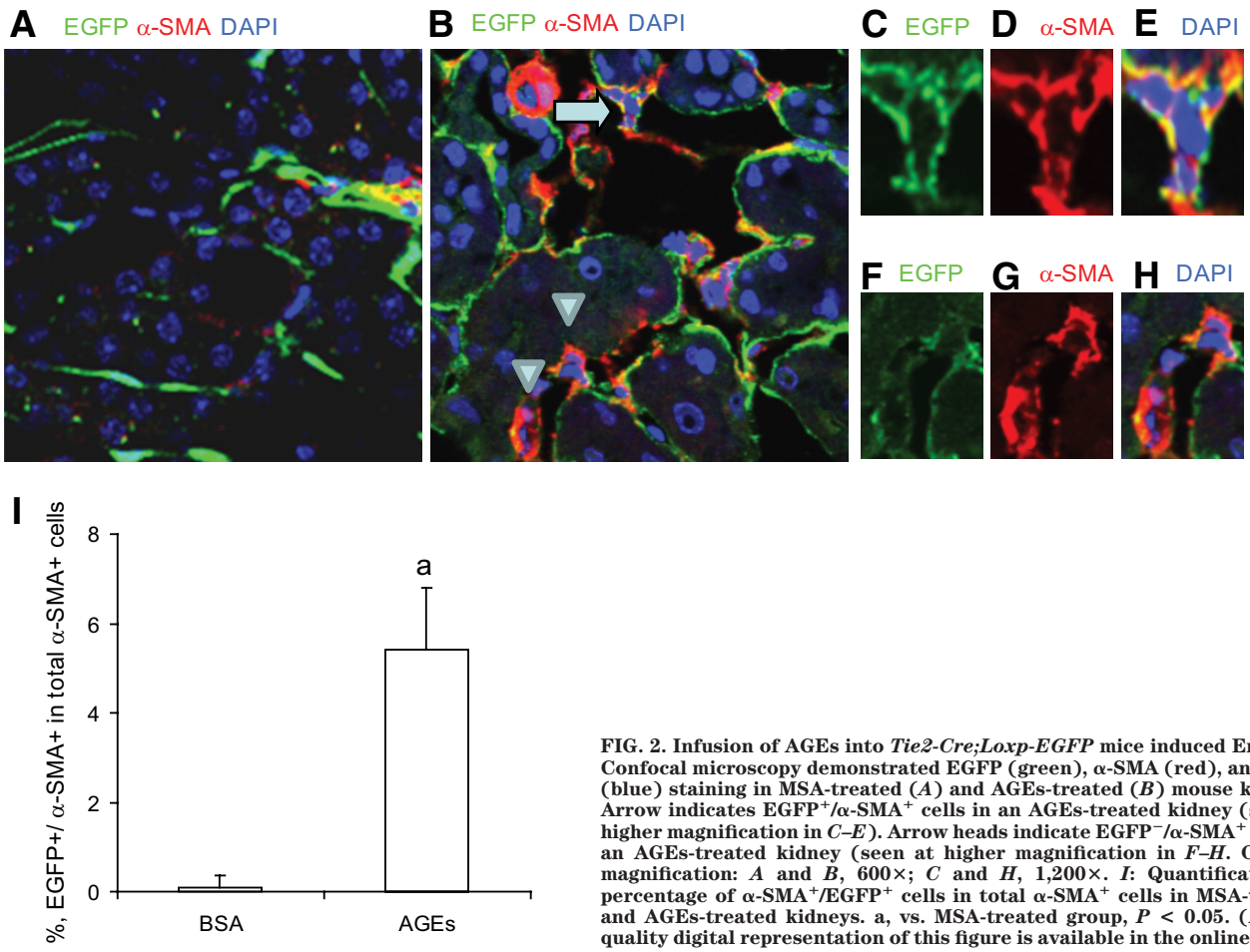

FIG. 2. Infusion of AGEs into *Tie2-Cre;Loxp-EGFP* mice induced EndoMT. Confocal microscopy demonstrated EGFP (green), α-SMA (red), and DAPI (blue) staining in MSA-treated (*A*) and AGEs-treated (*B*) mouse kidneys. Arrow indicates EGFP$^+$/α-SMA$^+$ cells in an AGEs-treated kidney (seen at higher magnification in *C–E*). Arrow heads indicate EGFP$^-$/α-SMA$^+$ cells in an AGEs-treated kidney (seen at higher magnification in *F–H*. Original magnification: *A* and *B*, 600×; *C* and *H*, 1,200×. *I*: Quantification of percentage of α-SMA$^+$/EGFP$^+$ cells in total α-SMA$^+$ cells in MSA-treated and AGEs-treated kidneys. a, vs. MSA-treated group, $P < 0.05$. (A high-quality digital representation of this figure is available in the online issue.)

tant to STZ-induced renal fibrosis and tubulointerstitial fibrosis in UUO models (25–27). Recently, Jinnin et al. (28) showed that a specific inhibitor of Smad3 (SIS3) inhibited Smad3 phosphorylation and reduced a transforming growth factor (TGF)-β1–induced fibrotic response in fibroblasts (10). We also demonstrated that SIS3 can abolish TGF-β1–induced EndoMT in mouse pancreatic microvascular endothelial cells (MMECs) (10). Whether SIS3 can inhibit AGE-induced EndoMT in vitro and in vivo remains to be explored.

In the present study, we hypothesized that AGEs can induce EndoMT and that blockade of RAGE-Smad3 cross-talk not only abrogates AGE-induced EndoMT but also retards the early development of renal fibrosis in STZ-induced diabetic mice. AGE-induced EndoMT was examined in MMECs and in an endothelial lineage–traceble mouse line (*Tie2-Cre;Loxp-EGFP*) while the efficacy of SIS3 was tested in AGE-induced EndoMT in MMECs and in mice with STZ-induced diabetes.

RESEARCH DESIGN AND METHODS

B6.Cg-Tg(Tek-cre)12F1v/J mice (stock no. 004128) and B6.Cg-Tg(ACTB-Bgeo/GFP)21Lbe/J mice (stock no. 004178) were purchased from the The Jackson Laboratories (Bar Harbor, ME). Male C57BL/6J mice (20–25g) were obtained from Monash Animal Services, Monash University, Australia. *α-SMA/EYFP* (enhanced yellow fluorescent protein) mice were kindly provided by Dr. James Lessard (Cincinnati Children's Hospital Medical Centre, Cincinnati, OH). In *α-SMA/EYFP* mice, EYFP expression is driven by the α-SMA promoter/enhancer and is expressed not only in smooth muscle cells but also in renal myofibroblasts. The isolation and culture of mouse renal CD31$^+$/EYFP$^-$ cells has previously been described (10). All animal experiments were performed with the approval of a Monash University Animal Ethics Committee and adhered to the *Australian Code of Practice for the Care and Use of Animals for Scientific Purposes*.

The generation of RAGE-null mice and induction of diabetes in RAGE-null and wild-type mice were described previously (13). Kidneys from 16- and 32-week-old diabetic and nondiabetic mice were used for periodic acid-Schiff (PAS) staining and confocal microscopy analysis.

Tie2-Cre;Loxp-EGFP mice were generated by cross-breeding B6.Cg-Tg(Tek-cre)12F1v/J mice with B6.Cg-Tg(ACTB-Bgeo/GFP)21Lbe/J mice. For the time course study, diabetes was induced in *Tie2-Cre;Loxp-EGFP* mice ($n = 12$) at 8 weeks of age by intraperitoneal administration of 50 μg/g STZ (Sigma-Aldrich, St. Louis, MO) for five consecutive days. Control *Tie2-Cre;Loxp-EGFP* mice ($n = 6$) received daily intraperitoneal injections of normal saline for 5 days. Mice were killed 1 and 3 month(s) after the onset of diabetes. Blood, urine, and kidney tissue were analyzed for biochemical parameters and renal histology. Urine in the bladder was collected for urinary albumin excretion once the mice were killed. The albumin-to-creatinine ratio was measured with Albuwell M and Creatinine Companion (Exocell, Philadelphia, PA).

A preliminary experiment was performed to determine the effective dose range of SIS3 in STZ-induced diabetic kidney disease. Diabetes was induced in male C57BL/6J mice by intraperitoneal injection of STZ as described above. One month after the onset of diabetes, mice were divided into four groups ($n = 3$) and given two intraperitoneal injections of 1, 2.5, or 5 μg/g body weight SIS3 or vehicle with a 5-h interval and then killed 1 h after the second injection for examination of the levels of renal Smad2 and Smad3 phosphorylation. Immunoprecipitation and western Blotting demonstrated that 2.5 μg/g SIS3 was sufficient to achieve more than 90% inhibition of phosphorylation of Smad3, compared with the vehicle-treated group, without obvious side effects. Therefore, in the main study, to test the beneficial role of SIS3, 4 weeks after onset of diabetes mice were treated with the same volume of vehicle or 2.5 mg · kg^{-1} · day^{-1} SIS3 delivered by implantation of an Alzet (Durect Corp., Cupertino, CA) osmotic pump for 8 weeks. By the experimental end point, mice were killed and blood, urine, and kidney tissue were collected for analysis.

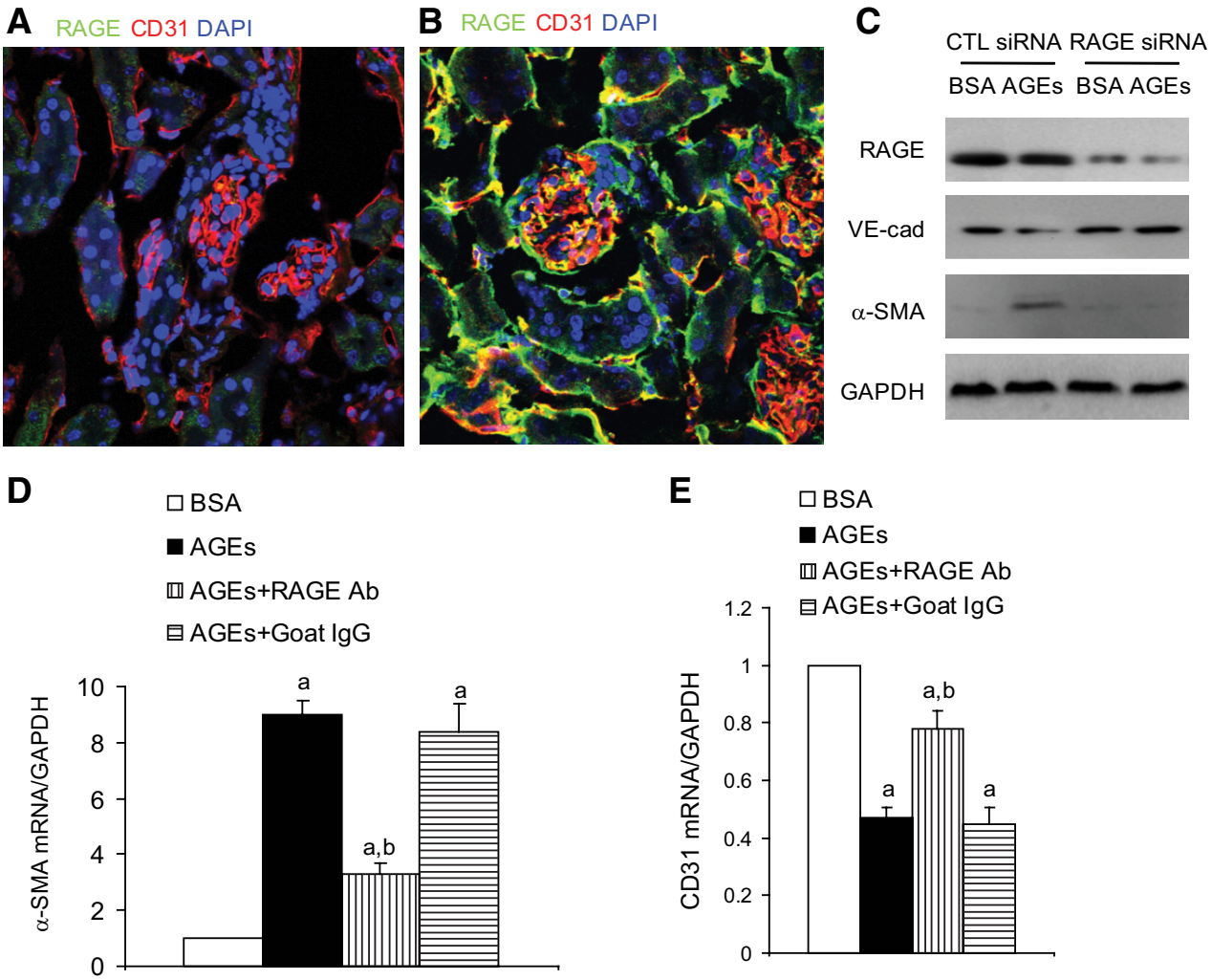

FIG. 3. AGE-induced EndoMT was RAGE-mediated in MMECs. Confocal microscopy demonstrated the expression of RAGE (green), CD31 (red), and DAPI (blue) in kidney 1 month after administration of either normal saline (*A*) or STZ (*B*). Original magnification for *A* and *B*, 600×. *C*: Mouse renal endothelial cells were treated with control siRNA (CTL siRNA) and RAGE siRNA for 24 h and then stimulated with BSA or AGEs for 48 h. Western blotting demonstrated the expression of RAGE, VE-cadherin (VE-cad), α-SMA, and GAPDH. *D* and *E*: Real-time PCR demonstrated mRNA levels of α-SMA (*D*) and CD31 (*E*) in MMECs after culture with BSA, AGEs, AGEs plus goat anti-RAGE neutralizing antibody or AGEs plus goat IgG for 24 h. a, vs. BSA, $P < 0.05$; b, vs. AGEs and AGEs plus goat IgG, respectively, $P < 0.05$. (A high-quality digital representation of this figure is available in the online issue.)

AGEs and mouse serum albumin infusion study. AGEs (10 μg · g^{-1} · day^{-1}; Sigma) or mouse serum albumin (MSA) (10 μg · g^{-1} · day^{-1}; Sigma) was administered into male *Tie2-Cre;Loxp-EGFP* mice ($n = 3$) for 1 month by osmotic micropumps. To test whether SIS3 can block EndoMT in vivo, MSA (10 μg · g^{-1} · day^{-1}), AGEs (10 μg · g^{-1} · day^{-1}) plus vehicle, or AGEs (10 μg · g^{-1} · day^{-1}) plus SIS3 (2.5 mg · kg^{-1} · day^{-1}) were administered into male *Tie2-Cre;Loxp-EGFP* mice ($n = 3$) for 1 month by separate osmotic micropumps. By the experimental end point, mice were killed and kidney tissues were collected for analysis.

Histology and confocal microscopy. The following antibodies were used for immunofluorescence studies: rat anti-CD31(BD Biosciences, San Diego, CA), rabbit anti–Von Willebrand factor (vWF) (Dako, Glostrup, Denmark), mouse anti–α-SMA conjugated with cyanine three (Sigma-Aldrich), rat anti–VE-cadherin (eBioscience, San Diego, CA), rabbit anti–phosphorylated Smad3 (Novus Biologicals, Littleton, CO), rabbit anti-fibronectin (Sigma-Aldrich), goat anti–collagen IV, goat anti–rabbit Alexa Fluor 555 conjugate, goat anti–rat Alexa Fluor 647 conjugate, and chicken anti–goat 647 conjugate (Invitrogen). Goat anti-RAGE neutralizing antibody and mouse anti–TGF-β1 neutralizing antibody (R&D Systems) were also used. Sections were counterstained with DAP) to visualize nuclei. Sections were analyzed with an Olympus Fluoview 1000 confocal microscope (Olympus, Tokyo), FV10-ASW software (version 1.7; Olympus), and oil Uplan filter 60× objective (NA 1.25; Olympus) at 2×, 3×, or 6× digital zoom. Channels were acquired sequentially. Contrast and brightness of the images were further adjusted using Image J (rsbweb.nih.gov/ij). The degree of tubulointerstitial fibrosis was measured in 40 randomly selected high-power fields (×600) in each animal using Image J software by analyzing the percentage of the total cortical area accounted for by immunostaining for α-SMA, collagen IV, or fibronectin. All scoring was performed blind on coded slides.

Quantitation of myofibroblasts of endothelial cell origin. Enhanced green fluorescent protein (EGFP)$^+$/α-SMA$^+$ cells were counted in renal cortex. Five cortical fields were analyzed at 600× magnification in each of five sections from each kidney. The number of endothelial cell–origin myofibroblasts per millimeter squared of cortex (excluding glomeruli) (EGFP$^+$/α-SMA$^+$ cells/millimeter squared of cortex) was determined, as was the percentage of α-SMA$^+$/EGFP$^+$ cells in total α-SMA$^+$ cells.

MMEC culture. MMECs were cultured as previously described (9). AGEs (Sigma-Aldrich) were added at concentrations of 1, 5, and 25 μg/ml to the cell cultures for 3 and 7 days in chamber slides and 3, 6, and 24 h in 6-well plates, with 25 μg/ml BSA used as the control. In blocking studies, MMECs were pretreated with goat anti-RAGE neutralizing antibody (4 μg/ml), mouse anti–TGF-β1 neutralizing antibody (4 μg/ml), normal goat immunoglobulin G (IgG) (4 μg/ml), normal mouse IgG (4 μg/ml), and SIS3 (2 μmol/l; Sigma Aldrich) or vehicle (DMSO) for 30 min; then, AGEs were added for different periods of time as described above. The treated cells were subsequently subjected to immunoprecipitation/Western blotting and real-time PCR.

RAGE, TGF-β receptor 1, Smad2, and Smad3 knockdown. Control siRNA (category no. 12935-200), RAGE siRNA (category no. MSS218607), TGF-β receptor 1 siRNA (category no. RSS355451), Smad2 siRNA (category no. MSS206406), and Smad3 siRNA (category no. MSS206422) were purchase

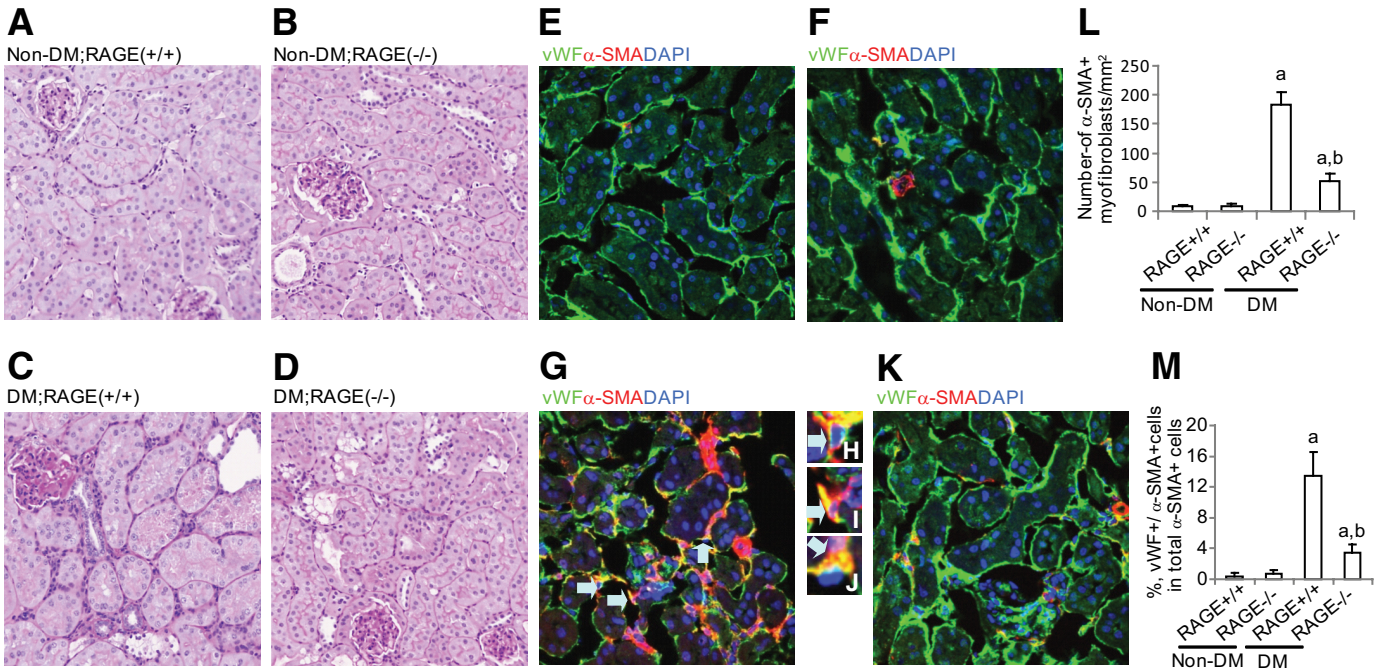

FIG. 4. RAGE-mediated EndoMT and diabetic (DM) renal fibrosis. PAS staining showed histological changes in RAGE–wild-type ($RAGE^{+/+}$) (*A* and *C*), RAGE-null ($RAGE^{-/-}$) (*B* and *D*), nondiabetic (*A* and *B*), and diabetic (*C* and *D*) kidneys at 32 weeks of age. Confocal microscopy demonstrated vWF (green), α-SMA (red), and DAPI (blue) in nondiabetic $RAGE^{+/+}$ (*E*), nondiabetic $RAGE^{-/-}$ (*F*), diabetic $RAGE^{+/+}$ (*G–J*), and diabetic $RAGE^{-/-}$ (*K*) kidneys. Original magnification: *A–D*, 400×; *E–G* and *K*, 600×; and *H–J*, 1800×. Quantification of number of α-SMA^+ renal interstitial myofibroblasts (*L*) and percentage of $vWF^+/\alpha\text{-}SMA^+$ cells in total α-SMA^+ cells (*M*). a, vs. nondiabetic kidneys, $P < 0.05$; b, vs. diabetic $RAGE^{+/+}$ kidneys, $P < 0.05$. (A high-quality digital representation of this figure is available in the online issue.)

from Invitrogen. For cell culture studies, mouse renal endothelial cells or MMECs were transfected in triplicate with RAGE siRNA, TGF-β receptor 1 siRNA, Smad2 siRNA, and Smad3 siRNA or control siRNA using lipofectamine 2000. Twenty-four hours following transfection, the transfected cells were subjected to BSA or AGEs stimulation for 30 mins, 24 h, or 48 h. Cells were harvested for immunoblotting or real-time PCR analysis.

RNA extraction and real-time PCR. Total RNA from kidneys or MMECs was isolated, and RT-PCR and real-time PCR were performed with an RT-PCR kit (Invitrogen) and SYBR Green PCR Reagents (Sigma). Primers were as follows: mouse CD31, 5′-aggcttgcatagagctccag and 5′-ttcttggtttccagctatgg; α-SMA, 5′-ctgacagaggcaccactgaa and 5′-gaaatagccaagctcag; mouse collagen IV, 5′aaagggagaaagaggcttgc and 5′ ctccctttgtaccgttgcat; mouse fibronectin, 5′gaagcaacgtgctatgacga and 5′atctagcggcatgaagcact; and mouse glyceraldehyde 3 phosphate dehydrogenase (GAPDH), 5′-cagatccacaacggatatattggg and 5′-catgacaactttggcattgtgg. Reaction specificity was confirmed by electrophoretic analysis of products before real-time PCR, and bands of expected size were detected. Ratios of CD31 to GAPDH, α-SMA to GAPDH, collagen IV to GAPDH, and fibronectin to GAPDH were calculated for each sample and expressed as means ± SD. The relative amounts of mRNA were calculated using the comparative Ct (ΔCt) method compared with GAPDH and are expressed as means ± SD.

Immunoprecipitation and Western blotting. Kidney and cell culture samples were sonicated and resuspended in 0.4 ml RIPA lysis buffer. Protein concentration estimations were performed with a detergent-compatible protein assay kit (Bio-Rad, Hercules, CA). Samples containing 500 μg total protein were immunoprecipitated with a rabbit anti-Smad3 antibody (Cell Signaling Technology, Danvers, MA) followed by Western blotting with mouse anti-phosphoserine (Calbiochem, Kilsyth, Victoria, Australia) or mouse anti-Smad3 (Santa Cruz Biotechnology, Santa Cruz, CA). Blots were then incubated with peroxidase-conjugated goat anti–rabbit IgG, goat anti–mouse IgG, or goat anti–mouse IgM (Sigma-Aldrich), and bound antibody was detected by ECL Plus (Amersham, Little Chalfont, U.K.) and captured by Fujifilm model LAS-3000 (Fujifilm Corporation). Densitometry analysis was performed with a Gel Pro analyzer (Media Cybernetics, Silver Spring, MD).

Statistical analysis. Data are presented as means ± SD, with statistical analyses performed using one-way ANOVA from GraphPad Prism 5.0 or two-way ANOVA if appropriate (GraphPad Software, San Diego, CA). Post-test Tukey's analysis was used when appropriate. A P value <0.05 was considered statistically significant.

RESULTS

AGEs induced EndoMT in MMECs and in *Tie2-Cre; Loxp-EGFP* mice. To investigate whether AGEs can induce EndoMT, we cultured MMECs in the presence of AGEs and unglycated BSA. MMECs have previously been shown to transdifferentiate into myofibroblasts in vitro upon TGF-β1 stimulation (10). Confocal microscopy (Fig. 1*A–C*) and real-time PCR (Fig. 1*D–G*) demonstrated that AGEs, but not BSA, induced de novo expression of α-SMA, a putative marker of myofibroblasts. Concurrently, MMEC expression of the endothelial cell markers VE-cadherin (protein) and CD31 (mRNA) were lost in a time- and dose-dependent fashion. To corroborate the findings in vivo, AGEs or MSA were administrated to *Tie2-Cre;Loxp-EGFP* mice by osmotic micropumps. In *Tie2-Cre;Loxp-EGFP* mice, expression of EGFP in renal endothelial cells persists despite subsequent phenotypic changes (10). Confocal microscopy demonstrated that by 1 month after AGEs infusion, $EGFP^+/\alpha\text{-}SMA^+$ cells were present in the renal interstitium but were not present in mice administered MSA (AGEs vs. MSA 5.4 ± 1.4 vs. 0.1 ± 0.3%; $P < 0.05$) (Fig. 2*A–I*). Thus, both in vitro and in vivo studies demonstrated the existence of AGE-induced EndoMT in microvascular endothelial cells.

RAGE-Smad3 cross-talk mediated AGE-induced EndoMT in MMECs. To investigate the expression of RAGE in renal endothelial cells, anti-RAGE and anti-CD31 antibodies were employed. Confocal microscopy demonstrated that the expression of RAGE was significantly increased in 1-month STZ-induced diabetic kidneys compared with normal saline-treated mouse kidneys (Fig. 3*A* and *B*). The colocalized expression of RAGE with CD31 demonstrated the significant upregulation of RAGE expression in diabetic renal endothelial cells both in glomer-

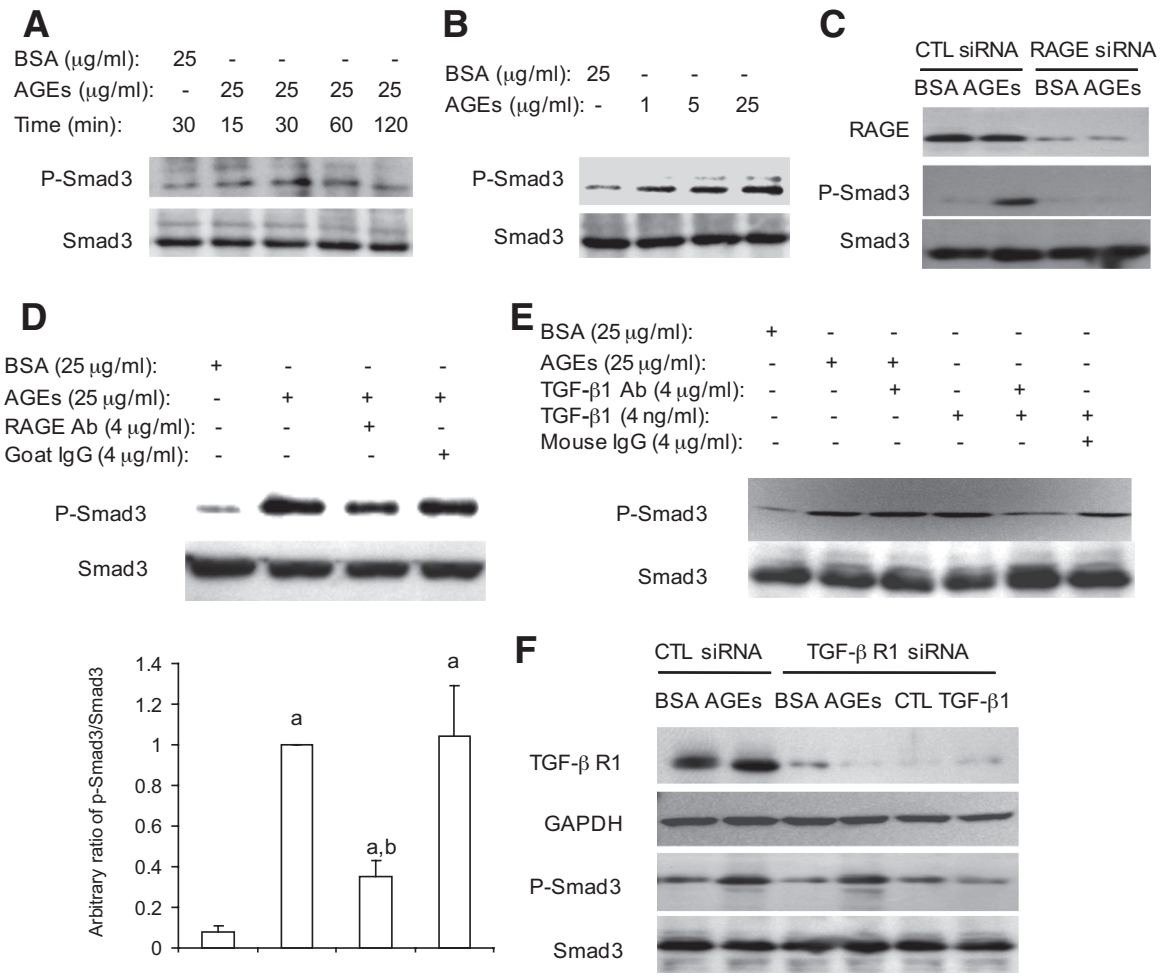

FIG. 5. AGE-induced activation of Smad3 was RAGE mediated in MMECs. MMECs were cultured in the presence of AGEs and BSA for 15–120 min or with different concentrations of AGEs for 30 min. Immunoprecipitation (IP) and Western blotting (WB) demonstrated the time course (*A*) and dose response (*B*) of Smad3 phosphorylation (p-Smad3) and total Smad3 levels in MMECs. *C*: MMECs were pretreated with control siRNA (CTL siRNA) or RAGE siRNA for 2 days and then cultured in the presence of BSA or AGEs for 30 min. Immunoprecipitation/Western blotting demonstrated RAGE, p-Smad3, and total Smad3 in MMECs. *D*: MMECs were pretreated with goat anti-RAGE neutralizing antibody or goat IgG for 30 min and then cultured in the presence of AGEs. *Upper panel*: Immunoprecipitation/Western blotting demonstrated Smad3 phosphorylation and total Smad3 in MMECs. *Lower panel*: quantitation of arbitrary ratio of Smad3 phosphorylation/Smad3 in three independent experiments. a, vs. BSA-treated group, $P < 0.05$; b, vs. AGEs or AGEs plus goat IgG, $P < 0.05$. *E*: MMECs were pretreated with mouse anti–TGF-β1 neutralizing antibody or mouse IgG for 30 min and then cultured in the presence of AGEs for 30 min. Immunoprecipitation/Western blotting demonstrated Smad3 Smad3 phosphorylation and total Smad3 in MMECs. *F*: MMECs were pretreated with control siRNA or TGF-β receptor 1 siRNA for 2 days and then cultured in the presence of AGEs for 30 min. Immunoprecipitation/Western blotting demonstrated TGF-β receptor 1, GAPDH, p-Smad3, and total Smad3 in MMECs.

uli and in peritubular capillaries (Fig. 3*A* and *B*). To investigate whether AGE-induced EndoMT involves signaling through RAGE, RAGE siRNA was employed. Western blotting demonstrated that knockdown of RAGE abolished AGE-induced loss of VE-cadherin and de novo expression of α-SMA in mouse endothelial cells (Fig. 3*C*). MMECs were also preincubated with goat anti-RAGE neutralizing antibody or goat IgG. Real-time PCR demonstrated that pretreatment with the anti-RAGE neutralizing antibody, but not control goat IgG, reduced AGE-induced α-SMA mRNA expression by 64% and inhibited loss of CD31 by 60% compared with AGEs treatment alone and cotreatment with AGEs and goat IgG (Fig. 3*D* and *E*). To further corroborate RAGE-mediated EndoMT in diabetes, diabetes was induced in RAGE-null and wild-type mice. PAS staining demonstrated that renal fibrosis was significantly reduced in RAGE-null diabetic kidney compared with RAGE–wild-type diabetic kidney (Fig. 4*A–D*). More importantly, confocal microscopy showed that the number of α-SMA$^+$ renal myofibroblasts and the percentage of vWF$^+$/α-SMA$^+$ cells in total α-SMA$^+$ cells were significantly lower in RAGE-null mouse kidney than in RAGE–wild type mouse kidney (Fig. 4*E–M*). This suggests that AGE-induced EndoMT occurs largely through RAGE. Next, we investigated whether AGEs can induce Smad3 activation and whether AGE-induced Smad3 activation occurs through RAGE. Immunoprecipitation/Western blotting demonstrated that incubation with AGEs induced Smad3 activation in a time- and dose-dependent fashion in MMECs (Fig. 5*A* and *B*). This AGE-induced Smad3 activation was reduced by 65% when MMECs were cultured in the presence of the anti-RAGE neutralizing antibody (Fig. 5*D*). When RAGE siRNA was employed in MMECs, this AGE-induced rapid Smad3 phosphorylation was almost abrogated (Fig. 5*C*). To further confirm RAGE-Smad3 cross-talk induced by AGEs, an anti–TGF-β1 neutralizing antibody and TGF-β receptor 1 siRNA were employed in MMECs. Western blotting demonstrated that the anti–TGF-β1 neutralizing antibody could block TGF-β1–induced but not AGE-induced rapid Smad3 activation (30

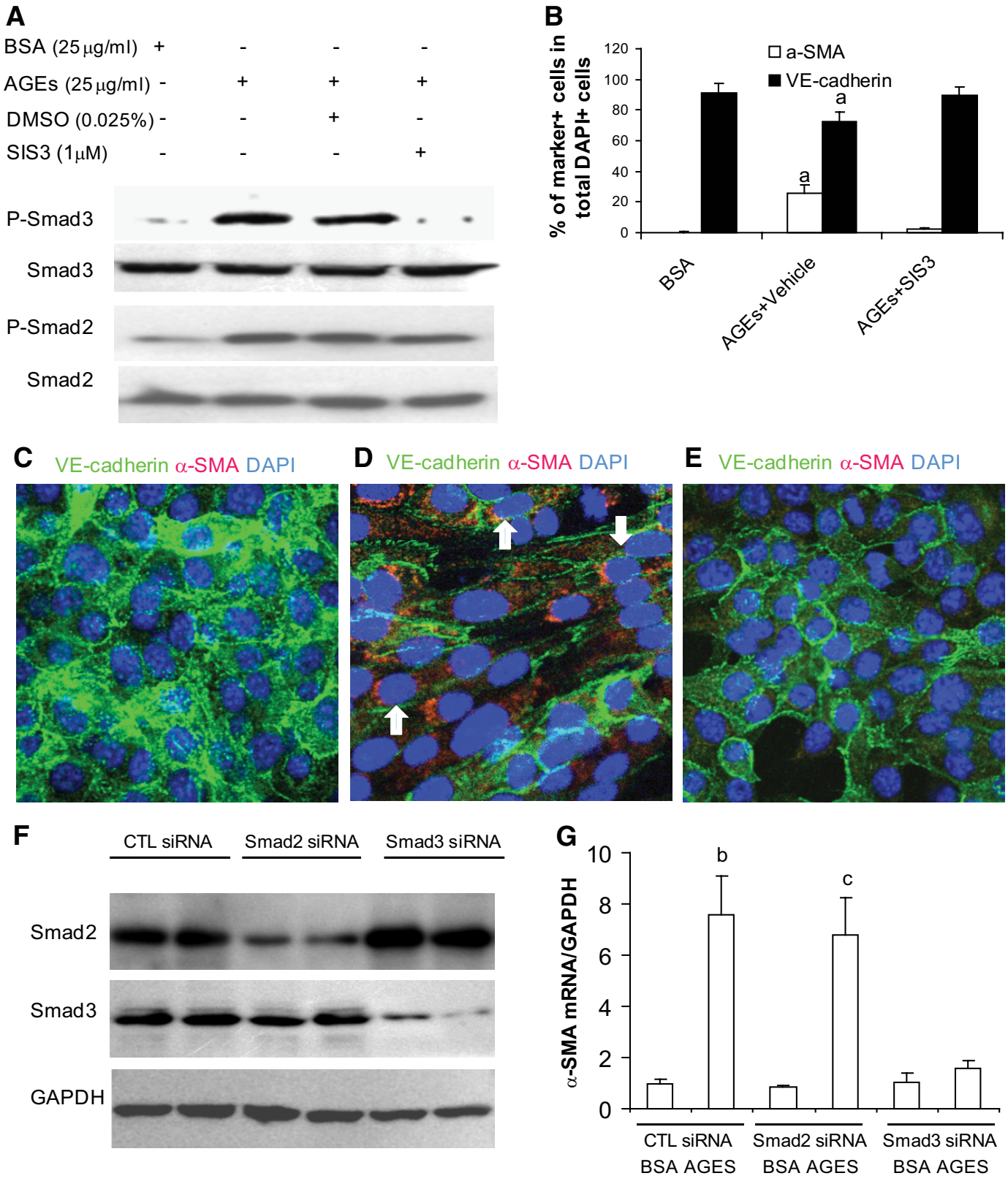

FIG. 6. SIS3 inhibited AGE-induced activation of Smad3 and EndoMT in MMECs. MMECs were pretreated with 1 μmol/l SIS3 or DMSO for 30 min and then cultured in the presence of 25 μg/ml AGEs for 30 min or 7 days. Immunoprecipitation/Western blotting demonstrated Smad3 phosphorylation (p-Smad3), Smad3, p-Smad2, and Smad2 at 30 min after AGEs stimulation in the presence of SIS3 (*A*). Confocal microscopy demonstrated the expression of VE-cadherin (green), α-SMA (red), and DAPI (blue) 7 days after incubation with BSA (*C*), AGEs plus DMSO (*D*), and AGEs plus SIS3 (*E*) in MMECs. Arrows indicate VE-Cadherin$^+$/α-SMA$^+$ cells. *B*: Quantitation of percentages of α-SMA– and VE-cadherin–positive cells in total DAPI-positive cells. a, vs. BSA-treated group or AGEs plus SIS3–treated group, $P < 0.05$. Original magnification 600×. *F* and *G*: MMECs were pretreated with control siRNA (CTL siRNA), Smad2 siRNA, or Smad3 siRNA for 2 days and then cultured in the presence of AGEs or BSA for 24 h. Western blotting demonstrated Smad2, Smad3, and GAPDH in MMECs (*F*), and real-time PCR showed α-SMA mRNA levels in MMECs (*G*). b, vs. BSA, $P < 0.05$. c, vs. BSA, $P < 0.05$. (A high-quality digital representation of this figure is available in the online issue.)

mins) (Fig. 5*E*). Western blotting also demonstrated that knockdown of TGF-β receptor 1 abrogated TGF-β1–induced but not AGE-induced rapid Smad3 activation (30 min) in MMECs (Fig. 5*F*). Thus, the experiment results demonstrate that RAGE-Smad3 cross-talk is a major pathway mediating AGE-induced Smad3 activation in MMECs.

SIS3 abrogated AGE-induced Smad3 activation and EndoMT in MMECs. SIS3 has previously been shown to inhibit Smad3 phosphorylation in fibroblasts (28), and we reported that SIS3 abolished TGF-β1–induced EndoMT in MMECs (10). To investigate whether SIS3 can block AGE-induced activation of Smad3, MMECs were pretreated with 1 μmol/l SIS3 for 30 mins. Immunoprecipitation/Western blotting demonstrated that SIS3 abolished AGE-induced phosphorylation of Smad3 but not Smad2, suggesting the specificity of SIS3 in vitro (Fig. 6*A*). Next, we investigated whether SIS3 could inhibit AGE-induced EndoMT in MMECs. Confocal microscopy demonstrated that pretreatment with SIS3 not only blocked AGE-induced de novo expression of α-SMA but also inhibited AGE-induced loss of VE-cadherin in MMECs (Fig. 6*B–E*), indicating the efficacy of SIS3 in inhibition of AGE-induced Smad3 phosphorylation and EndoMT in MMECs. To further differentiate the role of Smad2 and Smad3 in AGE-induced EndoMT, Smad2 siRNA and Smad3 siRNA were employed. Western blotting demonstrated that Smad2 siRNA and Smad3 siRNA significantly knocked down endogenous Smad2 and Smad3, respectively, in MMECs (Fig. 6*F*). Real-time PCR demonstrated that knockdown of Smad3 but not Smad2 almost abolished AGE-induced de novo expression of α-SMA in MMECs (Fig. 6*G*), suggesting the pivotal role of Smad3 in AGE-induced EndoMT.

SIS3 inhibited Smad3 activation in STZ-induced diabetic nephropathy in *Tie2-Cre;Loxp-EGFP* mice. Analysis of STZ-induced diabetic kidneys by immunoprecipitation/Western blotting identified substantial Smad3 phosphorylation 1 month after induction of diabetes. Levels of Smad3 phosphorylation remained elevated 3 months after STZ administration (Fig. 7*A*). Under a regime of multiple low-dose STZ injections, ~80% of the animals developed diabetes (29). Immunoprecipitation/Western blotting demonstrated that the level of Smad3 phosphorylation was not increased in STZ-injected nondiabetic mouse kidney compared with normal saline-injected and STZ-injected diabetic mouse kidneys (Fig. 7*B*), suggesting that the elevated Smad3 phosphorylation is associated with diabetes—not STZ. Confocal microscopy further confirmed a significant increase in levels of phosphorylated Smad3 in renal endothelial cells of diabetic mice compared with normal saline-injected mice (Fig. 7*E–I*). One month after the onset of STZ-induced diabetes, mice were given intraperitoneal injection of vehicle and different dosages of SIS3. Immunoprecipitation/Western blotting demonstrated that SIS3 blocked Smad3 but not Smad2 activation in STZ-induced diabetic mouse kidneys, suggesting the specificity of SIS3 in vivo (Fig. 7*C*). To explore whether SIS3 can inhibit Smad3 activation in STZ-induced diabetic nephropathy, SIS3 (2.5 $\mu g \cdot g^{-1} \cdot day^{-1}$) or the same volume of vehicle was administered to *Tie2-Cre;Loxp-EGFP* mice by osmotic micropumps for 2 months commencing 1 month after the administration of STZ. ImmunoprecipitationP/Western blotting demonstrated that after 2 months of SIS3 administration, Smad3 activation in STZ diabetic mice was almost abolished compared with high levels of Smad3 activation in kidneys of vehicle-injected mice (Fig. 7*D*). Confocal microscopy demon-

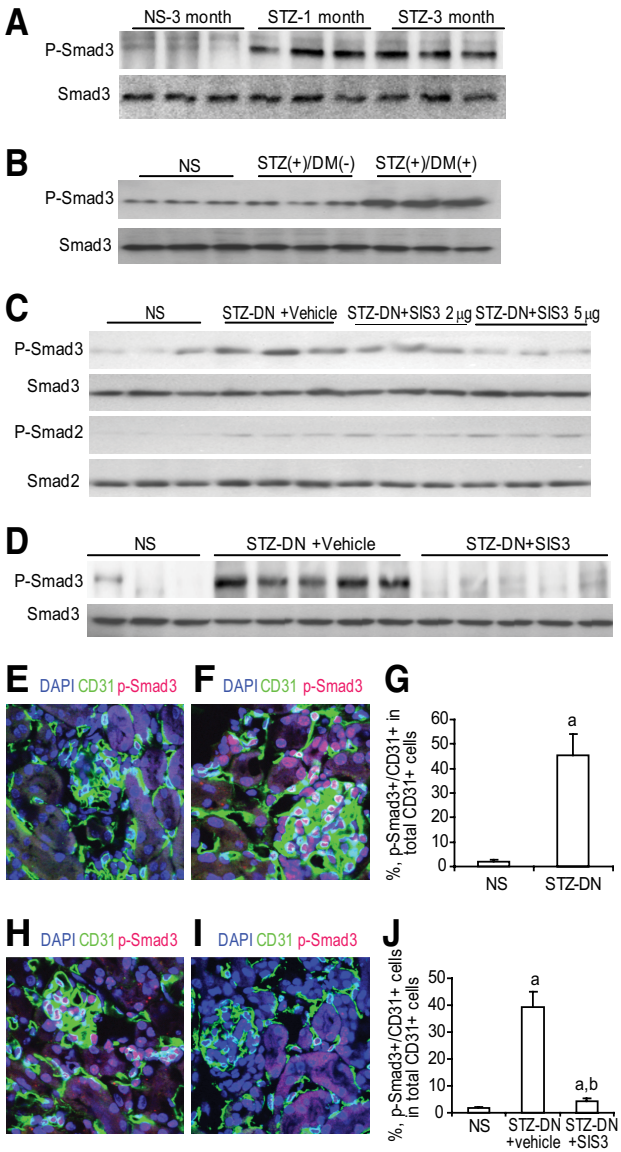

FIG. 7. SIS3 inhibited Smad3 activation in STZ-induced diabetic nephropathy. Immunoprecipitation/Western blotting demonstrated the time course of phosphorylated Smad3 (p-Smad3) and total levels of Smad3 in STZ-induced diabetic mouse kidneys and normal saline (NS)-treated kidneys (*A*) and p-Smad3 and total Smad3 in normal saline-treated, STZ-injected nondiabetic (STZ+/DM−) and STZ-injected diabetic (STZ+/DM+) mouse kidneys (*B*). *C*: One month after the onset of STZ-induced diabetes or normal saline treatment, diabetic mice were given intraperitoneal injection of vehicle and different dosages of SIS3. Immunoprecipitation/Western blotting demonstrated p-Smad3, total Smad3, p-Smad2, and total Smad2 in kidneys of mice with different treatments. *D*: Immunoprecipitation/Western blotting demonstrated p-Smad3 and total Smad3 in normal saline-treated mouse kidneys, STZ-induced diabetic nephropathy plus vehicle-treated mouse kidneys, and STZ-induced diabetic nephropathy plus SIS3-treated (2.5 $\mu g \cdot g^{-1} \cdot day^{-1}$) mouse kidneys. Confocal microscopy demonstrated CD31 (green), p-Smad3 (red), and DAPI (blue) staining in 1-month normal saline-treated kidney (*E*), 1-month STZ-induced diabetic kidney (*F*), 3-month STZ-induced diabetic nephropathy plus vehicle-treated mouse kidney (*H*), and 3-month STZ-induced diabetic nephropathy plus SIS3-treated mouse kidney (*I*). *G*: Quantitation of percentage of phosporylated Smad3–positive cells in total CD31-positive cells in 1-month normal saline-treated and STZ-injected diabetic kidneys. *J*: Quantitation of percentage of phosphorylated Smad3–positive cells in total CD31-positive cells in 3-month normal saline-treated and STZ-induced diabetic nephropathy plus vehicle-treated and STZ-induced diabetic nephropathy plus SIS3 treated kidneys. a, vs. normal saline, $P < 0.05$; b, vs. STZ-induced diabetic nephropathy plus vehicle-treated kidneys, $P < 0.05$. Original magnification: *C*, *D*, *F*, and *G*, 600×. (A high-quality digital representation of this figure is available in the online issue.)

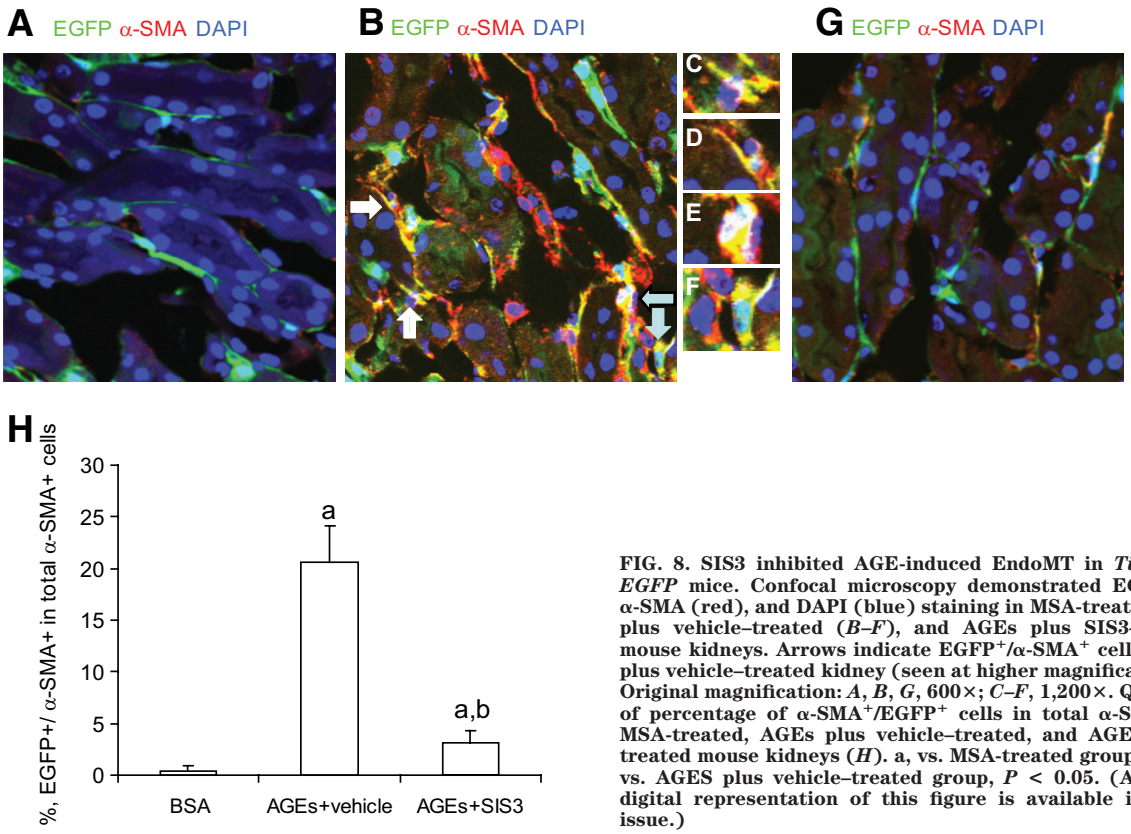

FIG. 8. SIS3 inhibited AGE-induced EndoMT in *Tie2-Cre;Loxp-EGFP* mice. Confocal microscopy demonstrated EGFP (green), α-SMA (red), and DAPI (blue) staining in MSA-treated (*A*), AGEs plus vehicle–treated (*B–F*), and AGEs plus SIS3–treated (*G*) mouse kidneys. Arrows indicate EGFP$^+$/α-SMA$^+$ cells in an AGEs plus vehicle–treated kidney (seen at higher magnification in *C–F*). Original magnification: *A*, *B*, *G*, 600×; *C–F*, 1,200×. Quantification of percentage of α-SMA$^+$/EGFP$^+$ cells in total α-SMA$^+$ cells in MSA-treated, AGEs plus vehicle–treated, and AGEs plus SIS3–treated mouse kidneys (*H*). a, vs. MSA-treated group, $P < 0.05$; b, vs. AGES plus vehicle–treated group, $P < 0.05$. (A high-quality digital representation of this figure is available in the online issue.)

strated that Smad3 activation in renal endothelial cells of STZ diabetic mice was inhibited by SIS3 (Fig. 7*H–J*), indicating the efficacy of SIS3 in vivo.

SIS3 reduced AGE-induced EndoMT and decreased EndoMT in STZ-induced diabetic nephropathy in *Tie2-Cre;Loxp-EGFP* mice. To investigate the effect of SIS3 on AGE-induced EndoMT in vivo, MSA, AGEs plus vehicle and AGEs plus SIS3 were administered into *Tie2-Cre;Loxp-EGFP* mice by osmotic pumps for 1 month. Confocal microscopy demonstrated that compared with vehicle treatment, SIS3 significantly inhibited AGE-induced EndoMT in *Tie2-Cre;Loxp-EGFP* mouse kidneys (Fig. 8*A–H*). Next, we examined the effects of SIS3 on EndoMT in STZ-induced diabetic nephropathy in *Tie2-Cre;Loxp-EGFP* mice. Confocal microscopy demonstrated that SIS3 reduced the percentage of EGFP$^+$/α-SMA$^+$ cells in total α-SMA$^+$ cells and the total number of α-SMA$^+$ cells in the renal interstitium compared with the vehicle-injected group (2.7 ± 0.8 vs. 14.2 ± 4.0% and 30.3 ± 10.5 vs. 158.7 ± 19.1 cells/mm^2, respectively; $P < 0.05$ (Fig. 9*A–N*). This suggests that SIS3 not only inhibited EndoMT but also reduced the accumulation of renal interstitial myofibroblasts.

Effects of SIS3 on the early development of renal fibrosis, macrophage infiltration, and renal function. Confocal microscopy and real-time PCR demonstrated that compared with vehicle treatment, SIS3 significantly reduced collagen IV (Fig. 10*A–C*, *G*, and *H*) and fibronectin (Fig. 10*D–F*, *G*, and *H*) expression in the glomeruli and tubulointerstitium of STZ-injected *Tie2-Cre;Loxp-EGFP* mice. This suggests that SIS3 retarded the early development of STZ-induced diabetic glomerulosclerosis and tubulointerstitial fibrosis. The renoprotective role of SIS3 was further confirmed by serum creatinine levels (STZ diabetic nephropathy plus SIS3 vs. STZ diabetic nephropathy plus vehicle 0.088 ± 0.013 vs. 0.11 ± 0.014 mg/dl; $P < 0.05$.) (Fig. 10*I*). However, SIS3 administration did not reduce proteinuria (urine albumin-to-creatinine ratio 221 ± 100 vs. 180 ± 78 μg/mg for STZ diabetic nephropathy plus SIS3 vs. STZ diabetic nephropathy plus vehicle, respectively; $P > 0.05$.) (Fig. 10*J*).

DISCUSSION

The present study showed that AGEs can induce EndoMT in vitro and in vivo and also demonstrated the central role of the RAGE-Smad3 signaling pathway in AGE-induced EndoMT. More importantly, the present study demonstrated the efficacy of SIS3 in the inhibition of EndoMT in vitro and in vivo and the renoprotective effects of SIS3 in STZ-induced diabetic nephropathy. Taken together, these findings suggest that EndoMT is a novel pathway leading to the development and progression of diabetic nephropathy and that SIS3 has therapeutic potential for diabetic renal disease.

Zeisberg et al. (9) and Li et al. (10) have recently demonstrated that EndoMT mediates the pathogenesis of diabetic renal fibrosis. In addition to TGF-β1 and TGF-β2, the present study further identified AGEs as inducers of EndoMT. Given the increasing evidence demonstrating a causal role for AGEs in the development of diabetes complications, AGE-induced EndoMT may also be an important mechanism in the pathogenesis of diabetic retinopathy and vasculopathy. Thus, blockade of AGE-induced EndoMT may have therapeutic benefit in retarding the progression of diabetes complications.

The interaction between AGEs and RAGE on endothelial cells initiates the activation of intracellular signaling pathways (15–23). AGEs also activate Smad2/3 signaling pathways through RAGE-MAPK cross-talk in nonendothe-

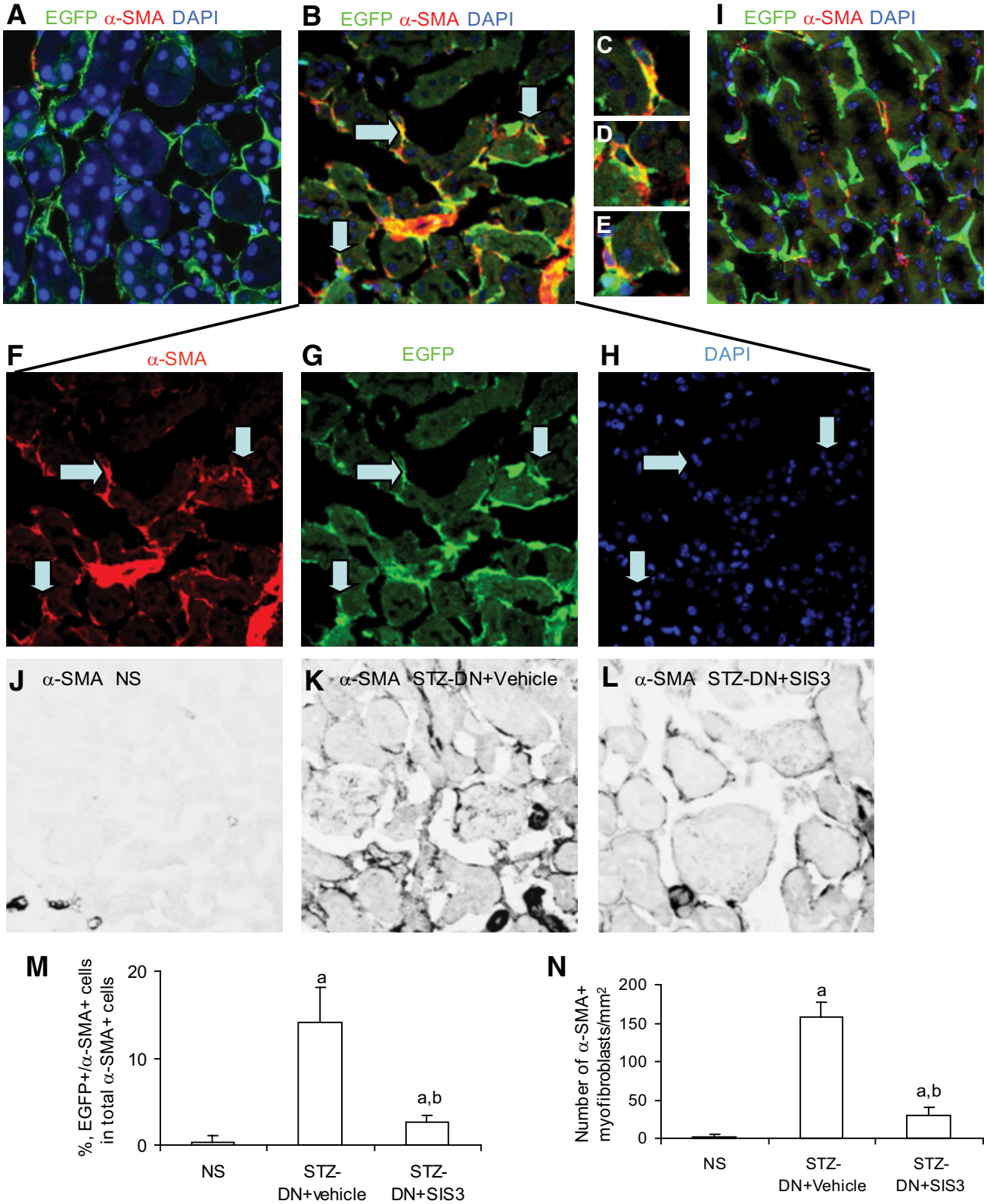

FIG. 9. SIS3 reduced EndoMT in STZ-induced diabetic nephropathy (DN) in *Tie2-Cre;Loxp-EGFP* mice. Confocal microscopy demonstrated EGFP (green), α-SMA (red), and DAPI (blue) in normal saline-treated kidney (*A*), STZ-induced diabetic nephropathy plus vehicle kidney (*B–H*), and STZ-induced diabetic nephropathy plus SIS3 mouse kidney (*I*). Arrows indicate EGFP$^+$/α-SMA$^+$ cells that are enlarged in *C–E*. *F*: α-SMA (red). *G*: EGFP (green). *H*: DAPI (blue). *B*: merged. Confocal microscopy demonstrated α-SMA staining in normal saline (NS)-treated (*J*), STZ-induced diabetic nephropathy plus vehicle-treated (*K*), and STZ-induced diabetic nephropathy plus SIS3-treated (*L*) mouse kidneys. Quantitation of percentage of EGFP$^+$/α-SMA$^+$ cells in total α-SMA$^+$ cells (*M*) and total number of α-SMA$^+$ myofibroblasts in normal saline, STZ-induced diabetic nephropathy plus vehicle and STZ-induced diabetic nephropathy plus SIS3 mouse kidneys (*N*). a, vs. normal saline, $P < 0.05$; b, vs. STZ-induced diabetic nephropathy plus vehicle, $P < 0.05$. Original magnification: *A*, *B*, *F–K*, 600×; *C–E*, 1,200×. (A high-quality digital representation of this figure is available in the online issue.)

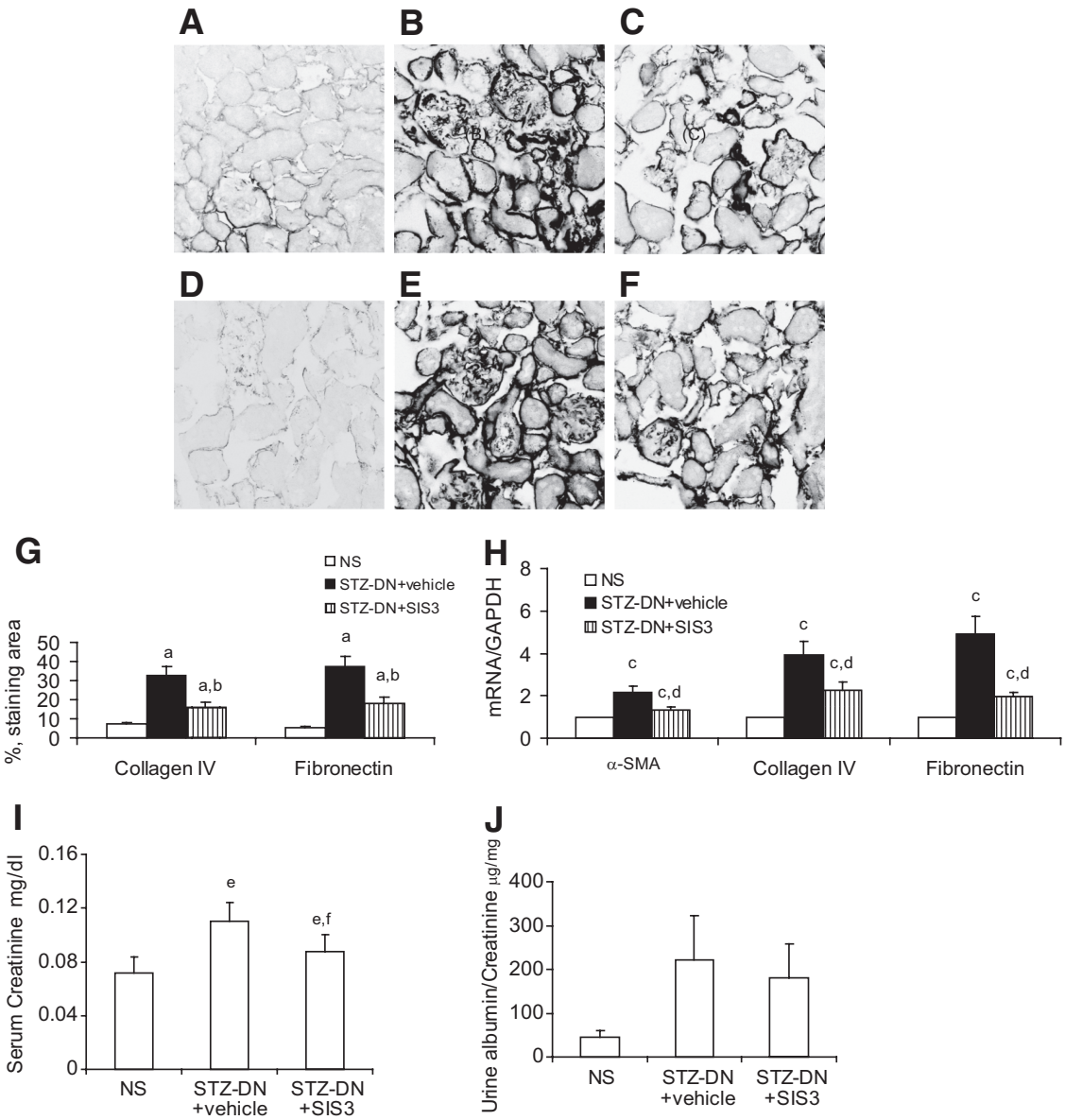

FIG. 10. SIS3 reduces renal fibrosis in diabetic nephropathy. Confocal microscopy demonstrated collagen IV (*A–C*) and fibronectin (*D–F*) immunostaining in normal saline (NS)-treated (*A* and *D*), STZ-induced diabetic nephropathy (STZ-DN) plus vehicle (*B* and *E*), and STZ-induced diabetic nephropathy) plus SIS3 (*C* and *F*) mouse kidneys. Original magnification 600×. *G*: Quantification of collagen IV and fibronectin staining in normal saline-treated, STZ-induced diabetic nephropathy plus vehicle-treated, and STZ-induced diabetic nephropathy plus SIS3-treated kidneys. a, vs. normal saline, $P < 0.05$; b, vs. STZ-diabetic nephropathy plus vehicle, $P < 0.05$. *H*: Real-time PCR demonstrated α-SMA, collagen IV, and fibronectin mRNA expression in normal saline, STZ-induced diabetic nephropathy plus vehicle, and STZ-induced diabetic nephropathy plus SIS3 mouse kidneys. c, vs. NS, $P < 0.05$; d, vs. STZ-induced diabetic nephropathy plus vehicle, $P < 0.05$. *I*: Serum creatinine in normal saline, STZ-induced diabetic nephropathy plus vehicle, and STZ-induced diabetic nephropathy plus SIS3 mouse kidneys. e, vs. NS, $P < 0.05$; f, vs. STZ-induced diabetic nephropathy plus vehicle, $P < 0.05$. *J*: Urine albumin/creatinine in normal saline, STZ-induced diabetic nephropathy plus vehicle, and STZ-induced diabetic nephropathy plus SIS3 groups. No significant differences were identified.

lial cells (24). The present findings demonstrate that AGEs can induce Smad3 activation in endothelial cells and that this Smad3 activation occurs largely through RAGE. Blockade of AGE-RAGE engagement or Smad3 activation inhibited AGE-induced EndoMT, indicating the essential role of RAGE-Smad3 cross-talk in AGE-induced EndoMT. Accordingly, RAGE-Smad3 cross-talk may be a therapeutic target for diabetic nephropathy.

SIS3 has been shown to inhibit Smad3 phosphorylation and abrogate TGF-β1–induced ECM production in fibroblasts (28). The present study demonstrated that SIS3 not only inhibited AGE-induced Smad3 activation and EndoMT in vitro but also abrogated Smad3 activation, decreased EndoMT, and retarded the progression of diabetic nephropathy in vivo. Again, these findings suggest that blockade of Smad3 phosphorylation may have therapeutic potential for diabetic nephropathy, although further studies are obviously required.

In addition to AGEs, other profibrotic mediators, such as TGF-β and connective tissue growth factor, are elevated by AGEs in renal cells and can activate Smad3. Smad3 is activated in a variety of renal cells besides endothelial cells, such as tubular epithelial cells, fibroblasts, and mesangial cells, which also contribute to renal fibrosis. SIS3 inhibits Smad3 activation in these renal cells. Therefore, the effect of SIS3 in the kidney is not only restricted to endothelial cells.

Clinical trials of RAS inhibitors in patients with both

type 1 and type 2 diabetes have shown protective effects on reducing renal and cardiovascular damage in patients with advanced diabetic nephropathy with proteinuria (30,31). However, large randomized clinical trials have revealed that inhibition of the RAS fails to prevent the development of early diabetic renal disease (5,32), suggesting that additional mechanism(s) may participate in the development of diabetic renal disease. The present findings demonstrated that AGEs induced EndoMT in vitro and in vivo and that blockade of Smad3 phosphorylation by SIS3 significantly reduced EndoMT, decreased glomerulosclerosis and tubulointerstitial fibrosis, and improved renal function. These findings suggest that EndoMT is a novel pathway leading to diabetic nephropathy and that SIS3 may constitute a new measure to treat patients with diabetic nephropathy.

Previous studies of Smad3 conditional knockout mice with STZ-induced diabetes (25,26) or renal pathology due to UUO (27) have demonstrated the essential role of Smad3 in both glomerulosclerosis and tubulointerstitial fibrosis. However, the role of Smad3 in proteinuria remains controversial. Fujimoto et al. (25) showed that compared with wild-type mice, proteinuria was significantly decreased in Smad3 knockout mice with STZ-induced diabetic nephropathy, while Wang et al. (26) demonstrated that Smad3 deficiency limited diabetic glomerulosclerosis without affecting albuminuria. We have previously reported that EndoMT occurs and contributes to early renal interstitial fibrosis independently of microalbuminuria (10). In the present study, SIS3 treatment did not attenuate albuminuria. However, all of the above studies investigated proteinuria in the early stages of experimental diabetic kidney disease. The effect of SIS3 on proteinuria in advanced diabetic nephropathy deserves investigation.

In the present study, the anti-RAGE neutralizing antibody and RAGE siRNA significantly inhibited AGE-induced EndoMT in both MMECs and mouse renal endothelial cells. Further, SIS3 almost completely blocked AGE-induced EndoMT in MMECs and in *Tie2-Cre;Loxp-EGFP* mouse kidneys. This suggests that RAGE is a major receptor involved in the induction of EndoMT while Smad3 plays an essential role in AGE-induced EndoMT. The administration of SIS3 to mice with STZ-induced diabetic nephropathy significantly reduced, but did not completely retard, the development of diabetic renal fibrosis, suggesting that other pathological factors, such as activation of p38MAPK (33,34), ERK (35,36), and protein kinase C (37,38); high glucose (39,40); and oxidative stress (41,42) may also be involved in the pathogenesis of diabetic nephropathy.

In conclusion, the present study identified a novel mechanism in which AGE-induced EndoMT occurs and contributes to the development of diabetic renal fibrosis. RAGE-Smad3 cross-talk plays a central role in AGE-induced EndoMT. SIS3 not only inhibits EndoMT but also prevents structural damage and provides renal functional protection. Blockade of EndoMT and RAGE-Smad3 cross-talk may provide a new strategy to retard the progression of diabetic nephropathy and other diabetes complications.

ACKNOWLEDGMENTS

This work was supported by the National Health and Medical Research Council (NHMRC) of Australia. J.L. is the recipient of a NHMRC Peter Doherty Postdoctoral Fellowship (2007–2009) and a NHMRC Career Development Award (2010–2013).

No potential conflicts of interest relevant to this article were reported.

Confocal imaging was performed at the Monash Micro-Imaging Facility at Monash University.

J.L. researched data and wrote, reviewed, and edited the manuscript. X.Q. researched data. J.Y. researched data. G.C. reviewed and edited the manuscript. S.D.R. contributed to the discussion. Y.Y. researched data. H.Y. researched data. J.F.B. reviewed and edited the manuscript.

REFERENCES

1. Kizu A, Medici D, Kalluri R. Endothelial-mesenchymal transition as a novel mechanism for generating myofibroblasts during diabetic nephropathy. Am J Pathol 2009;175:1371–1373
2. Lewis EJ, Hunsicker LG, Bain RP, Rohde RD. The effect of angiotensin-converting-enzyme inhibition on diabetic nephropathy. N Engl J Med 1993;329:1456–1462
3. Lewis EJ, Hunsicker LG, Clarke WR, Berl T, Pohl MA, Lewis JB, Ritz E, Atkins RC, Rohde R, Raz I, the Collaborative Study Group. Renoprotective effect of the angiotensin-receptor antagonist irbesartan in patients with nephropathy due to type 2 diabetes. N Engl J Med 2001;345:851–860
4. Brenner BM, Cooper ME, de Zeeuw D, Berl T, Pohl MA, Lewis JB, Ritz E, Atkins RC, Rohde R, Raz I, the Collaborative Study Group. Effects of losartan on renal and cardiovascular outcomes in patients with type 2 diabetes and nephropathy. N Engl J Med 2001;345:861–869
5. Mauer M, Zinman B, Gardiner R, Suissa S, Sinaiko A, Strand T, Drummond K, Donnelly S, Goodyer P, Gubler MC, Klein R. Renal and retinal effects of enalapril and losartan in type 1 diabetes. N Engl J Med 2009;361:40–51
6. Pedagogos E, Hewitson T, Fraser I, Nicholls K, Becker G. Myofibroblasts and arteriolar sclerosis in human diabetic nephropathy. Am J Kidney Dis 1997;29:912–918
7. Essawy M, Soylemezoglu O, Muchaneta-Kubara EC, Shortland J, Brown CB, Nahas AM. Myofibroblasts and the progression of diabetic nephropathy. Nephrol Dial Transplant 1997;12:43–50
8. Zeisberg EM, Tarnavski O, Zeisberg M, Dorfman AL, McMullen JR, Gustafsson E, Chandraker A, Yuan X, Pu WT, Roberts AB, Neilson EG, Sayegh MH, Izumo S, Kalluri R. Endothelial-to-mesenchymal transition contributes to cardiac fibrosis. Nat Med 2007;13:952–961
9. Zeisberg EM, Potenta SE, Sugimoto H, Zeisberg M, Kalluri R. Fibroblasts in kidney fibrosis emerge via endothelial-to-mesenchymal transition. J Am Soc Nephrol 2008;19:2282–2287
10. Li J, Qu X, Bertram JF. Endothelial-myofibroblast transition contributes to the early development of diabetic renal interstitial fibrosis in streptozotocin-induced diabetic mice. Am J Pathol 2009;175:1380–1388
11. Schmidt AM, Stern DM. RAGE: a new target for the prevention and treatment of the vascular and inflammatory complications of diabetes. Trends Endocrinol Metab 2000;11:368–375
12. Bucala R, Vlassara H. Advanced glycosylation end products in diabetic renal and vascular disease. Am J Kid Dis 1995;26:875–888
13. Myint KM, Yamamoto Y, Doi T, Kato I, Harashima A, Yonekura H, Watanabe T, Shinohara H, Takeuchi M, Tsuneyama K, Hashimoto N, Asano M, Takasawa S, Okamoto H, Yamamoto H. RAGE control of diabetic nephropathy in a mouse model: effects of RAGE gene disruption and administration of low–molecular weight heparin. Diabetes 2006;55:2510–2522
14. Oldfield MD, Bach LA, Forbes JM, Nikolic-Paterson D, McRobert A, Thallas V, Atkins RC, Osicka T, Jerums G, Cooper ME. Advanced glycation end products cause epithelial-myofibroblast transdifferentiation via the receptor for advanced glycation end products (RAGE). J Clin Invest 2001;108:1853–1863
15. Bierhaus A, Illmer T, Kasper M, Luther T, Quehenberger P, Tritschler H, Wahl P, Ziegler R, Muller M, Nawroth PP. Advanced glycation end product (AGE)-mediated induction of tissue factor in cultured endothelial cells is dependent on RAGE. Circulation 1997;96:2262–2271
16. Yan SD, Schmidt AM, Anderson GM, Zhang J, Brett J, Zou YS, Pinsky D, Stern D. Enhanced cellular oxidant stress by the interaction of advanced glycation end products with their receptors/binding proteins. J Biol Chem 1994;269:9889–9897
17. Schiekofer S, Andrassy M, Chen J, Rudofsky G, Schneider J, Wendt T, Stefan N, Humpert P, Fritsche A, Stumvoll M, Schleicher E, Haring HU, Nawroth PP, Bierhaus A. Acute hyperglycemia causes intracellular forma-

tion of CML and activation of ras, p42/44 MAPK, and nuclear factor-κB in PBMCs. Diabetes 2003;52:621–633
18. Huttunen HJ, Fages C, Rauvala H. Receptor for advanced glycation end products (RAGE)-mediated neurite outgrowth and activation of NF-κB require the cytoplasmic domain of the receptor but different downstream signaling pathways. J Biol Chem 1999;274:19919–19924
19. Taguchi A, Blood DC, del Toro G, Canet A, Lee DC, Qu W, Tanji N, Lu Y, Lalla E, Fu C, Hofmann MA, Kislinger T, Ingram M, Lu A, Tanaka H, Hori O, Ogawa S, Stern DM, Schmidt AM. Blockade of RAGE-amphoterin signaling suppresses tumour growth and metastases. Nature 2000;405:354–360
20. Stern DM, Yan SD, Yan SF, Schmidt AM. Receptor for advanced glycation endproducts (RAGE) and the complications of diabetes. Ageing Res Rev 2002;1:1–15
21. Wautier J-L, Schmidt AM. Protein glycation. A firm link to endothelial cell dysfunction. Circ Res 2004;95:233–238
22. Huttunen HJ, Rauvala H. Amphoterin as an extracellular regulator of cell motility: from discovery to disease. J Intern Med 2004;255:351–366
23. Nakagawa T, Sato W, Glushakova O, Heinig M, Clarke T, Campbell-Thompson M, Yuzawa Y, Atkinson MA, Johnson RJ, Croker B. Diabetic endothelial nitric oxide synthase knockout mice develop advanced diabetic nephropathy. J Am Soc Nephrol 2007;18:539–550
24. Li JH, Huang XR, Zhu HJ, Oldfield M, Cooper M, Truong LD, Johnson RJ, Lan HY. Advanced glycation end products activate Smad signaling via TGF-beta-dependent and independent mechanisms: implications for diabetic renal and vascular disease. FASEB J 2004;18:176–178
25. Fujimoto M, Maezawa Y, Yokote K, Joh K, Kobayashi K, Kawamura H, Nishimura M, Roberts AB, Saito Y, Mori S. Mice lacking Smad3 are protected against streptozotocin-induced diabetic glomerulopathy. Biochem Biophys Res Commun 2003;305:1002–1007
26. Wang A, Ziyadeh FN, Lee EY, Pyagay PE, Sung SH, Sheardown SA, Laping NJ, Chen S. Interference with TGF-beta signaling by Smad3-knockout in mice limits diabetic glomerulosclerosis without affecting albuminuria. Am J Physiol Renal Physiol 2007;293:F1657–F1665
27. Sato M, Muragaki Y, Saika S, Roberts AB, Ooshima A. Targeted disruption of TGF-beta1/Smad3 signaling protects against renal tubulointerstitial fibrosis induced by unilateral ureteral obstruction. J Clin Invest 2003;112:1486–1494
28. Jinnin M, Ihn H, Tamaki K. Characterization of SIS3, a novel specific inhibitor of Smad3, and its effect on transforming growth factor-beta1-induced extracellular matrix expression. Mol Pharmacol 2006;69:597–607
29. Kanetsuna Y, Takahashi K, Nagata M, Gannon MA, Breyer MD, Harris RC, Takahashi T. Am J Pathol 2007;170:1473–1484
30. Lewis EJ, Hunsicker LG, Bain RP, Rohde RD, the Collaborative Study Group. The effect of angiotensin-converting-enzyme inhibition on diabetic nephropathy. N Engl J Med 1993;329:1456–1462
31. Hollenberg NK, Raij L. Angiotensin-converting enzyme inhibition and renal protection: an assessment of implications for therapy. Arch Intern Med 1993;153:2426–2435
32. Jerums G, Panagiotopoulos S, Premaratne E, Power DA, MacIsaac RJ. Lowering of proteinuria in response to antihypertensive therapy predicts improved renal function in late but not in early diabetic nephropathy: a pooled analysis. Am J Nephrol 2008;28:614–627
33. Komers R, Lindsley JN, Oyama TT, Cohen DM, Anderson S. Renal p38 MAP kinase activity in experimental diabetes. Lab Invest 2007;87:548–558
34. Adhikary L, Chow F, Nikolic-Paterson DJ, Stambe C, Dowling J, Atkins RC, Tesch GH. Abnormal p38 mitogen-activated protein kinase signalling in human and experimental diabetic nephropathy. Diabetologia 2004;47:1210–1222
35. Haneda M, Koya D, Kikkawa R. Cellular mechanisms in the development and progression of diabetic nephropathy: activation of the DAG-PKC-ERK pathway. Am J Kidney Dis 2001;38(Suppl. 1):S178–S181
36. Lin CL, Wang FS, Kuo YR, Huang YT, Huang HC, Sun YC, Kuo YH. Ras modulation of superoxide activates ERK-dependent fibronectin expression in diabetes-induced renal injuries. Kidney Int 2006;69:1593–1600
37. Wu D, Peng F, Zhang B, Ingram AJ, Kelly DJ, Gilbert RE, Gao B, Krepinsky JC. PKC-beta1 mediates glucose-induced Akt activation and TGF-beta1 upregulation in mesangial cells. J Am Soc Nephrol 2009;20:554–566
38. Meier M, Menne J, Haller H. Targeting the protein kinase C family in the diabetic kidney: lessons from analysis of mutant mice. Diabetologia 2009;52:765–775
39. Li JH, Huang XR, Zhu HJ, Johnson R, Lan HY. Role of TGF-beta signaling in extracellular matrix production under high glucose conditions. Kidney Int 2003;63:2010–2019
40. Wu L, Derynck R. Essential role of TGF-beta signaling in glucose-induced cell hypertrophy. Dev Cell 2009;17:35–48
41. Forbes JM, Coughlan MT, Cooper ME. Oxidative stress as a major culprit in kidney disease in diabetes. Diabetes 2008;57:1446–1454
42. Cooper ME. Pathogenesis, prevention, and treatment of diabetic nephropathy. Lancet 1998;352:213–219